Journal of Hydrology 605 (2022) 127296

Contents lists available at ScienceDirect

Journal of Hydrology

journal homepage: www.elsevier.com/locate/jhydrol

Research papers

Impacts of agricultural expansion on floodplain water and sediment budgets in the Mekong River

Edward Park [a,*], Huu Loc Ho [b], Doan Van Binh [c,d], Sameh Kantoush [c], Danielle Poh [a], Enner Alcantara [e], Sophal Try [c,f], Yunung Nina Lin [g]

[a] National Institute of Education, Earth Observatory of Singapore and Asian School of the Environment, Nanyang Technological University, Singapore
[b] Water Engineering and Management, School of Engineering and Technology, Asian Institute of Technology, Thailand
[c] Disaster Prevention Research Institute, Kyoto University, Japan
[d] Master Program in Water Technology, Reuse and Management, Vietnamese-German University, Vietnam
[e] Department of Environmental Engineering, São Paulo State University, Brazil
[f] Faculty of Hydrology and Water Resources, Institute of Technology of Cambodia, Cambodia
[g] Institute of Earth Science, Academia Sinica, Taiwan

ARTICLE INFO

This manuscript was handled by J Simunek, Editor-in-Chief, with the assistance of Todd C. Rasmussen, Associate Editor

Keywords:
Floodplain
Sedimentation
Land use land cover change
Human impacts
Cambodia
Mekong

ABSTRACT

In this paper, we address the impact of agricultural expansion on hydrological patterns of water and sediment budget in one of the largest floodplains along the Cambodian Mekong since the 1980s, using field (water level, discharge, sediment, rainfall, and groundwater level) and remote sensing (land use, surface suspended sediment) data, and numerical simulations. Specifically, while both the surface suspended sediment concentration and water level in the Mekong River around Kampong Cham and Neak Luong decreased, the floodplain seasonal water storage increased. In addition, the rate of sediment input from the river to the floodplain was almost constant throughout the studied period. The investigation of the floodplain's annual sediment budget, however, reveals a significant drop during the analyzed period, mainly due to the decreased sediment trapping rate (66% in the 1980s to 46% in the 2010s). Currently, a good amount of sediment bypass the floodplain and return back to the river. The observed hydrological patterns in the floodplain could have been triggered by the agricultural expansion that has increased surface erodibility (due to removals of primary vegetation) and lowered the land surface elevation (due to groundwater extraction). Despite the well-known impacts of the hydropower dams on the Mekong Delta hydrological conditions, particularly the reduction of sediment reaching the delta due to sediment trapping by dam reservoirs, our observations point to new and more localized driving factors of sediment deficit in floodplain: agricultural expansion. Finally, we used 2D hydrodynamic simulation (Telemac-2D) to visualize the processes of water routing and sedimentation in the floodplain accounting for land cover change since the 1980s. The floodplain hydrology reported in this paper is an unexplored environmental consequence of agricultural expansion in the lower Mekong. Geomorphologically, this study presents a peculiar case of floodplain showing how agricultural expansion can diminish the role of a floodplain as a sediment sink through decreasing the trapping rate.

1. Introduction

Along with rich water resources from the Mekong River, Cambodia has been developing its economies around agriculture, especially rice production exports. Currently, 65% of the entire labour force in Cambodia are engaged in rice production activities, contributing approximately 25% to the national gross domestic product (Cramb et al., 2020). However, the nation's irrigation capacity is limited and has only been able to irrigate 10 % of its rice crops. The rainfed lowland rice is still the most common cultivation system (Cramb et al., 2020; Erban & Gorelick 2016). Most Cambodian rice crops, therefore, are grown between May and November with ample surface water resources. Evidently, it is not the case for the dry season, which pushes the farmers towards exploiting the groundwater resources (Sok & Choup, 2017). As a result, on-site irrigation systems through sinking tube wells have been extensively used to draw groundwater to feed these rice fields during the

* Corresponding author.
E-mail address: edward.park@nie.edu.sg (E. Park).

https://doi.org/10.1016/j.jhydrol.2021.127296
Received 1 August 2021; Received in revised form 3 October 2021; Accepted 27 November 2021
Available online 14 December 2021
0022-1694/© 2021 The Author(s). Published by Elsevier B.V. This is an open access article under the CC BY license (http://creativecommons.org/licenses/by/4.0/).

dry seasons. Sok & Choup (2017) observed that more than 80% of the total groundwater extracted in Cambodia has ended up fueling agricultural activities, and the trend continues to rise over the years. In the Prey Veng province, for instance, the number of tube wells for irrigation had grown from 1,600 to 25,000 in the last decade (iDE, 2005).

Even though groundwater has been abundantly available in most areas of the lowland plains of Cambodia, especially around Tonle Sap Lake, promoting extensive groundwater use entails multiple environmental issues challenging the sustainable development of the region (Cramb et al., 2020). For instance, during the withdrawal, pore spaces within subsurface materials are reduced, causing the multiple layers of sediments to be compacted and ultimately lead to land subsidence (Erban et al., 2014). One of the most notable evidence was reported by Sok (2017) and Chen et al. (2019) in that excessive groundwater extraction around Angkor Wat could have been responsible for the sinking of this world heritage site. Poorly planned groundwater extraction could also intensify arsenic contamination via lowered water table (Erban et al., 2013; Winkel et al., 2011).

In the case of Prey Veng and Svey Rieng in Cambodia being the focus of this study, the drawdown exceeded the recharge rate, and the overall decline in groundwater levels from 1996 to 2008 was critically remarkable (Johnston et al., 2013). As a result, the unplanned overexploitation of groundwater has triggered a series of environmental consequences. This includes a declining water table, which makes it harder and costlier to lift, exacerbating land subsidence and arsenic contamination (Erban et al., 2013; Sok and Choup, 2017; Winkel et al., 2011). From the *trans*-catchment perspective, the water resources of these Cambodian floodplains are also vulnerable to multiple external pressures. Among these, the operation of upstream hydropower dams and the ever-intensifying riverbed mining activities could directly affect the available water resources by reducing the chronicle inundation frequencies of the floodplains (Park et al., 2020; Park et al., 2021a; Park et al., 2021b). Such a decrease of the natural supply of water to the floodplains would consequently lead to the disruption of the livelihoods of millions of agricultural habitats and, ultimately, the regional food security (e.g. Binh et al., 2020a; Eslami et al., 2019; Loc et al., 2017; Loc et al., 2021a; Loc et al., 2021b; Loc et al., 2021c among others).

Although the unfavourable outcomes from the proliferation of mechanized groundwater irrigation pumps have been well-documented in previous studies, either in the region (Erban et al., 2013; Erban & Gorelick, 2016) or in the broader Asia such as India or China (e.g. Shah et al., 2007), what distinguishes the case of Cambodian floodplains are the novel impacts of agricultural expansion-driven extensive groundwater extraction on floodplain water and sediment budgets. On the one hand, the seasonal water extents and flood frequencies along the largest Cambodian Mekong floodplain (close to Phnom Penh) have constantly increased over the past few decades (since the 1980s), according to the data by Pekel et al. (2016). On the other hand, the water levels and surface suspended sediment concentration (*SSSC*) in the Mekong River constantly exhibit decreasing trends in the respective period related to the upstream dam constructions and riverbed mining (Binh et al., 2020b; Binh et al., 2021; Ng & Park, 2021). Such seemingly contradictory phenomena, however, could have been attributed to the enhanced water accommodation capacity of the floodplain (as shown in Fig. 1A) because of the subsided land surfaces, which is in turn, caused by groundwater extraction and surface erosion. Interestingly, in the beginning stages of our investigation (Section 3.1), we found that against the increased water fluxes into the floodplain and stationary sediment inflows, the sediment storage, i.e. the annual budget, still decreases significantly over the same period of time. We proceeded to hypothesize that it is the decline of surface roughness driven by the agricultural expansion that has significantly decreased the sediment trapping in the floodplain over recent years.

In this paper, we aim to address this hydrological pattern in the largest floodplain in Cambodian Mekong and to identify the root cause of the phenomena. We focused on this floodplain as a case study site

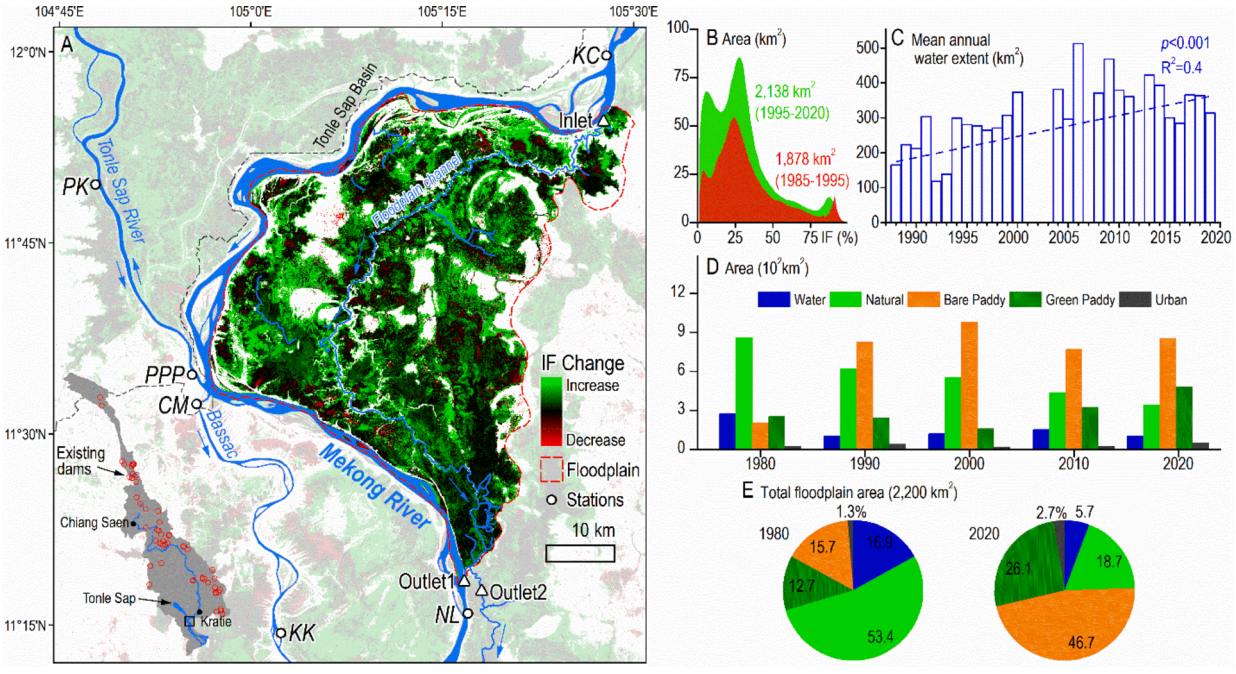

Fig. 1. Study area and the floodplain land cover change. A: The floodplain focused on in this study (bounded by a red dashed line). Hydrological inlet and outlets of the floodplain are shown (and the major floodplain channel that connects the two), as well as gauge stations along the Mekong. Water Occurrence Change Intensity change over the past 35 years is shown (data from Pekel et al., (2016)). The inset map shows the Mekong Basin and existing dams. Station abbreviation: Kampong Cham (*KC*), Phnom Penh Port (*PPP*), Chaktomuk (*CM*), Prek Kdam (*PK*) and Neak Luong (*NL*). B: Extent of floodplain area by inundation frequency for the two periods: 1985–1995 and 1995–2020. C: Average total flooded area within the floodplain calculated from Landsat data and its increasing trend. D and E: Mapped land cover change in the floodplain since the 1980s with methods expounded on in Section 2.4. (For interpretation of the references to colour in this figure legend, the reader is referred to the web version of this article.)

because it is representative of a cultivated floodplain system in the Cambodian Mekong. The floodplain has recently experienced agricultural expansion along with intensifying groundwater extraction and is also under direct impact of other environmental pressures regulating the river hydrology, such as dams and sand mining. We analyzed hydrological data (water level and discharge) at multiple gauge stations around the floodplain, reconstructed time series *SSSC* data at virtual gauge stations using field-calibrated optical remote sensing data, and then calculated water and sediment budgets. Agricultural expansion on the floodplain has been mapped since the early 1980s, which is corroborated by groundwater level data over 17 monitoring wells. Since our analysis of floodplain water and sediment budgets is based on hydrological data in the Mekong River main channel, we incorporated results from two-dimensional hydrodynamic simulation (Telemac-2D) to visualize the floodplain water routing patterns and sedimentation processes accounting for the land cover changes during the studied periods.

2. Data and methods

2.1. Hydrological data and trend analysis at gauge stations

Daily water level and discharge (*Q*) data for the four stations along the lower Mekong River in Cambodia: Kampong Cham (*KC*), Chaktomuk (*CM*), Prek Kdam (*PK*) and Neak Luong (*NL*) from 1980 to 2020 were obtained from the Mekong River Commission (MRC) (Fig. 1). These stations were chosen to calculate the water and sediment budget of the floodplain. Some of these stations had missing *Q* records between 2002 and 2020, and for those cases, daily *Q* were estimated by the rating curves (between water level and *Q*). *KC* is located around 10 km upstream from the inlet, where the Mekong water is transferred to the floodplain through channelized flow (Fig. 1). *NL* is located around 5 km downstream from Outlet1. The water export from the floodplain happens via Outlet1 or Outlet2, and there is no floodplain channel that connects the river and the floodplain between *KC* and *NL* (verified through the maximum inundation area map by Pekel et al. (2016)). Both inlet and outlet are permanent channels that remain connected even during the dry season. The Tonle Sap River connects the Mekong River to the Tonle Sap Lake. The flow direction of the river is reversed seasonally – toward the lake and river during wet and dry seasons, respectively. *CM* is located on the Bassac River, close to Phnom Penh. First, trends of hydrological time series were analyzed using the seasonal Mann-Kendall's test (MK, at 95% confidence level), a robust, nonparametric procedure in which Kendall's *tau* with time as the covariate is computed by the user-defined season (Helsel & Hirsch, 1992). Median slopes of all ranked seasonal regression slopes are used to estimate the slope for the trend's magnitude. Temporal autocorrelation was not accounted for because we examined the trends with the period of record (McBride, 2005). We tested the time series at 95% confidence level, and *p*-values and Kendall's *tau* are reported in section 3. Hydrological data used in this study is summaried in Table 1.

2.2. Calculating floodplain water budget

Floodplain water budget was computed using *Q* data at the gauge stations and other hydrological variables, i.e. rainfall, evapotranspiration (*ET*) rate and *Q* at Outlet2, using the following equation:

$$Seasonal\ water\ budget = Q_{KC} - Q_{CM} - Q_{NL} \pm Q_{PK} - (Q_{Outlet2} + Rainfall - ET) \quad (1)$$

where Q_x denotes the mean monthly discharge at the station × and $Q_{Outlet2}$ (not a station) is the discharge at Outlet2 along the floodplain channel. Other than Q_{KC} and Q_{NL} along the Mekong mainstream, there are several other variables used in the annual water budget computation. Q_{CM} representing the Bassac River's discharge – a distributary of the Mekong – which we subtracted from Q_{KC}; Q_{PK} representing the discharge added to the floodplain water budget during the falling season when water flows from Tonle Sap to the Mekong, and vice versa during the rising season. $Q_{Outlet2}$ is an atypically long meandering ~90 km branch that merges back to the Mekong main channel in Vietnam close to the border. $Q_{Outlet2}$ was estimated by the Acoustic Doppler Current Profiler (ADCP) survey data that we obtained in 2017 along the Vam Nao Channel, a geomorphologically similar floodplain channel in the Mekong Delta located approximately 30 km downstream from the Cambodian border. This floodplain channel with Outlet2 has the comparable sinuosity (index = 1.54), reach channel slope (~6.5 cm/km), stability (almost no migration was confirmed through visual inspection of Google Earth historical imagery during 1985–2019) and is constructed by similar fine sediment materials (Hackney et al., 2020); hence we consider that the w/d ratio of the two channels should be analogous. Manning's equation (Manning et al., 1890) was used to estimate the flow velocity of the floodplain channel as follow:

$$v = \frac{R^{\frac{2}{3}} \times S^{\frac{1}{2}}}{n} \quad (2)$$

where *R* is a hydraulic radius estimated using mean width (approximately 100 m measured from the 0.5 m resolution Digital Globe Image) and mean depth of the floodplain channel, and *S* is the slope, calculated from the ADCP data at the Vam Nao channel. Daily total rainfall data from 1980 to 2020 (at ~ 5 km resolution) is obtained from the Climate Hazards Group InfraRed Precipitation with Station data (CHIRPS) (Funk et al., 2015), and then total monthly rainfall landed on the floodplain was calculated. *ET* in the lower Mekong was obtained from Zhou et al. (2006) at 3–4 mm/day (averaged potential evapotranspiration over the lower Mekong). Consumption of water by paddy is not included in the budget because it does not affect hydrological input or output in the floodplain, rather it is partially accounted for in the *ET* term.

2.3. Estimating suspended sediment concentration based on field survey data, and the floodplain sediment budget

SSSC along the four virtual stations was estimated based on Landsat

Table 1
Hydrological data used in this study from gauge stations, altimetry stations, and their resolution and availability.

Station	Data availability				
	Water level (*WL*)[b]	Discharge (*Q*)	*SSSC*[d]	Rainfall	Groundwater level
KC, *PPP*, *PPB/CM*, *NL*[a]	1980–2020 (daily)	1980–2020 (daily)[c]	1987–2020 (~16-day)	–	–
Floodplain channel	2010–2018 (monthly)[d]	–	–	1980–2020 (daily; floodplain)	–
P.24/P.15	–	–	–	–	1998–2010 (monthly)

[a] Station locations: *KC* (11°58′8.91″N, 105°27′58.23″E), *PPP* (11°34′37.13″N, 104°55′43.29″E), *PPB* (11°32′44.35″N, 104°56′40.23″E) and *NL* (11°16′10.21″N, 105°16′46.42″E).
[b] Source: Mekong River Commission (MRC).
[c] 2002 onward estimated using a rating curve of the five previous years at respective stations. It should be noted that by MRC the rating curve of the stations in the main channel are re-calibrated at least once a year (number of times depends on station) through cross-section survey of the gauge station cross section.
[d] Source: Database for Hydrological Time Series of Inland Waters (DAHITI) (Schwatke et al., 2015).

data. Landsat 4–8 Level-2 atmospherically-corrected surface reflectance product since 1987 at 30 m resolution was downloaded from USGS Earth Explorer (a total of 647 images). First, we developed a reflectance-*SSSC* calibration model along the lower Mekong. Two field measurements of the *SSSC* in the Mekong River were used for calibration: 1) *SSSC* data around Phnom Penh Port (*PPP*) by Lu et al. (2014) collected between May 2008 to May 2011 (N = 32); and 2) *SSSC* data along the Mekong River in Vietnam (between Tan Chau and My Thuan – for location see Park et al., (2021)) collected between December 2020 and January 2021 (N = 23). Surface sediment was collected through surface water sampling using a 500 ml bottle, filtered with the Cellulose acetate membranes (0.45 μm), and weighted after drying 24 h. For the Landsat data, we used the red band (centred around 0.655 μm) which is constantly sensitive to the level of surface sediment concentration in inland turbid waters (Doxaran et al., 2002; Park and Latrubesse, 2014). A 7 × 7 pixel mask centered on the field measurement site was delineated, and median reflectance was computed after filtering out outlier pixels (i.e. greater than 2 standard deviations) to minimize the sensor noise. The remaining qualified pixels were used to build a regression model in which the slope is statistically significant at 95% confidence level (Fig. 2). Using this field-calibrated reflectance-*SSSC* model, *SSSC* time series since 1978 were estimated over the four virtual stations (529 < N < 1,308). Here we consider that most *Qs* that we calculate in this study is dominantly washload composed of mostly silt and clay, as verified by Hackney et al. (2020) and our own field survey data (<2% sand, Fig. 2B).

Estimated *SSSC* was incorporated with *Q* data to estimate the sediment fluxes (*Qs*) at each four stations as below:

$$Qs = SSSC_T \times Q_T \times k \tag{3}$$

where $SSSC_T$ and Q_T denotes *SSSC* and *Q* on a specific date *T*, while *k* is a conversion factor. The seasonal sediment budget of the floodplain was then calculated by the following equation:

$$Seasonal\ sediment\ budget = Qs_{KC} - Qs_{CM} - Qs_{NL} \pm Qs_{PK} - Qs_{Outlet2} \tag{4}$$

where Qs_x denotes the annual *Qs* at the station *x*. We verified through visual inspection of high-resolution images in Google Earth that there is no additional sediment input or output for the floodplain other than the fluxes through identified inlet or outlet in this study.

2.4. Mapping agricultural expansion and dry season NDVI using Landsat data

Land use and land cover change over the floodplain since the 1970s has been mapped based on Landsat data (at 30 m) on the Google Earth Engine (GEE) cloud-based platform. We used Level-1 Terrain Precision (L1TP) calibrated top-of-atmosphere (TOA) reflectance image (path 126 and row 52) that has been corrected for the atmospheric effects through the Landsat Ecosystem Disturbance Adaptive Processing System (LEDAPS) (Masek et al., 2012). Images with cloud cover and the shadows exceeding 25% were masked out. Random forest, after generating a classifier (trees) based on bootstrapped samples of training data within each image (Breiman, 1999), was used to classify the pixels into five classes: water, natural vegetation, bare paddy, green paddy and urban (classes defined by local expert knowledge).

Based on the same Landsat product on GEE, dry season Normalized Difference Vegetation Index (*NDVI*) was used to identify vegetation growth, and from there we made inferences to groundwater extraction activities. NDVI is defined as follows:

$$NDVI = (NIR - Red)/(NIR + Red) \tag{5}$$

while *NIR* and *Red* denote Near Infrared and Red bands, respectively. Since the positive *NDVI* values represent green vegetation (from grassland to dense forest toward 1), we computed the average value over the floodplain during the dry season (December-May) since the 1980s. The reasoning for this is that since double cropping is a predominant agricultural practice in this part of Cambodia (Ear et al., 2017; IRRA, 2010), farmers exploit groundwater to irrigate crops during the dry season (FAO, 2015) when floodplain recharges from both limited rainfall and the low Mekong water inflow (Ear et al., 2017; IRRA, 2010; Kwak et al., 2015). Without exploiting groundwater resources in the dry season when both the meteorological and fluvial hydrological inputs are limited, most of the floodplain land should have remained dry (barren land and dry soil) that normally yields lower NDVI values (i.e. NDVI < 0).

2.5. Groundwater level trend examination and field controls

The groundwater data level used in this study was provided by the International Development Enterprises (IDE). Provincial scale data of groundwater usage (total extraction rates and % out of domestic usage) has been supplied from Sok & Choup (2017). In this study, we considered groundwater level data from 17 wells, mostly within the Prey Veng and Kandal Provinces, of which the groundwater level data were measured once per month from 1996 to 2008 (see Section 3.2. for location). Using the groundwater level decline rates from the monitoring wells measured (relatively well-distributed across the study area), we created a heatmap via ordinary Kriging to signify the spatial patterns of groundwater level declines. For illustration purpose, monthly water

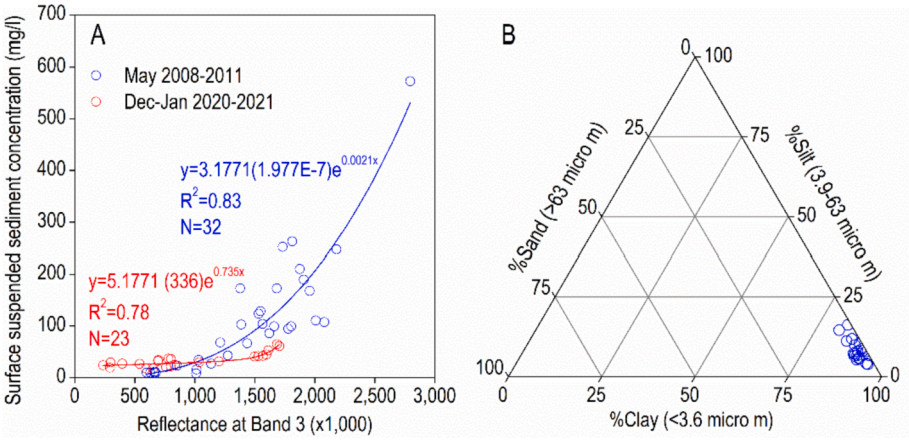

Fig. 2. Remote sensing model and grain size distribution. A: Surface reflectance-*SSSC* calibration model developed using two different *SSSC* samples (standard errors in the parenthesis). The slope of the two calibration models were statistically different after Analysis of Covariance test (ANCOVA, *p*-value < 0.01 at 95% confidence level), and also the ranges of two samples are largely different (ANCOVA is a widely used statistical testing that measures the significance of the two regression models). We used the calibration model derived from the sample collected 2008–2011 (e.g. Lu et al., 2014), which presented sufficiently large variability (approximately 500–2,700 mg/l) to capture the seasonal dynamics of both *SSSC* and surface reflectance. B: Grain size distribution results of 20 bucket samples (20 L) collected during the field survey in December 2020 and January 2021. Collected bucket waters were settled over 20 h before removing 80% of the upper water layer and then completely dried before obtaining the results via laser particle scanner (Fritsch Analysette-22).

level time series from two wells *P.24* (measured) and *P.15* (estimated from the ratio between *P.24* obtained from the interpolated map), are plotted. To verify the temporal change of groundwater level, we employed the Mann-Kendall test as described above. Lastly, photo-documentary evidence showing the consequences of the groundwater extraction in the study area, such as land subsidence, was collected from various sources online (in Khmer, keywords used

2.6. 2D hydrodynamic modelling of floodplain sedimentation

We used a coupled Telemac-2D and Sisyphe model of the Telemac Mascaret System to simulate spatial distribution patterns of sedimentation in the floodplain. The Telemac-2D model is used to simulate hydrodynamics, solving the depth-averaged Saint-Venant equations, while the Sisyphe model (Villaret, 2010; Villaret et al., 2013) simulates sediment transport and bed evolution by solving a two-dimensional advection–diffusion and the Exner equations as below (Exner, 1920; Exner, 1925; Pablo, 2018):

$$\frac{\partial hC}{\partial t}+\frac{\partial hUC}{\partial x}+\frac{\partial hVC}{\partial y}=\frac{\partial}{\partial x}\left(h\varepsilon_s\frac{\partial C}{\partial x}\right)+\frac{\partial}{\partial y}\left(h\varepsilon_s\frac{\partial C}{\partial y}\right)+E-D \quad (6)$$

where, C is the depth-averaged concentration (% volume); U and V are the depth-averaged velocities in x and y-directions (m/s), respectively; ε_s is the turbulent diffusivity of the sediment, related to the eddy viscosity $\varepsilon_s = \nu_t/\sigma_c$; σ_c is the Schmidt number (=1.0); ω_s is settling velocity (cm/s); E and D are the erosion and deposition rates, respectively, which are estimated by the equation below for bed elevation:

$$(1-\lambda)\frac{\partial z_b}{\partial t}+(E-D)=0 \quad (7)$$

where λ is the bed porosity; z_b is the bed level (m).

In the advection–diffusion equations, only suspended sediment is considered because sediment in the floodplain is mainly transported in the suspension mode (Hung et al. (2014)). Also, bedload contributes only 1–3% of the total load in the lower Mekong in Cambodia (Hackney et al., 2020). We internally coupled the Telemac-2D model with the Sisyphe model, by which hydrodynamic parameters solved by the Telemac-2D model are sent to the Sisyphe model to estimate bed evolution. The updated bed elevations are sent back into the Telemac-2D model to repeat the simulation cycles. During the flood season (June to November), the channelized flows from the Mekong River to the floodplain (via the inlet, Fig. 1 is the dominant source of the floodplain water and sediment budgets. An unstructured triangle mesh of 300 m was generated by a finite element method, totalling approximately 53,000 elements. We imposed daily discharge and *SSSC* at the upstream boundary (i.e. the floodplain Inlet) and free flow and sediment at the downstream boundary (i.e. the Outlet1).

The model was calibrated and validated against the flood data (June-November) in 2000, representing one of the most extreme floods that occurred during the investigated period. We performed a hot-start simulation, which was simulated for seven days using constant discharge and *SSSC* at the boundaries to obtain a steady condition. Then the results were used as initial conditions for the main simulations. The floodplain geometry was obtained from the Multi-Error Removed Improved-Terrain (MERIT) DEM (Yamazaki et al., 2017), where the elevation of the alluvial plain part of the floodplain (excluding uplands) ranged mostly from 1 to 12 m above EGM96 reference geoid (including floodplain ridges). The model was calibrated by tuning various parameters, including friction coefficient, velocity diffusivity (10^{-6} m/s) (for the Telemac-2D model), critical shear stress for erosion (0.15 N/m^2), critical shear velocity for deposition (0.03 m/s), settling velocity (6.6×10^{-5} m/s), and Krone-Partheniades erosion constant (1×10^{-6} kg/s/m^2) (for the Sisyphe model). The initial distribution of the Manning coefficient (n) was estimated from the 2000 land use map using the method described by Acrement, (1989). The Landsat-derived *SSSC* values at 30 random locations within the floodplain were compared to the simulated values to evaluate the model performance (validation). The goodness of the model was assessed by the coefficient of determination (R^2), and root mean square error (RMSE). After that, we simulated sedimentation in the floodplain driven by land use change from 1995 to 2015 by changing the Manning coefficient accordingly. Lastly, the simulated volume of sediment deposited in the floodplain each year is compared with the sediment budget (in mass, tons) using the porosity of silt and clay.

3. Results and discussion

3.1. Trends of floodplain water and sediment budgets

We first assessed the trends of discharge, *WL* and *SSSC* at the two stations (*KC* and *NL*, inlet and outlet, respectively). When computing the water and sediment budgets of the floodplain (in the next section), we used mainly these two inlet/outlet stations because there are no river-floodplain hydrological interactions along the Mekong reach between *KC* and *NL* (confirmed through visual inspections of the Global Surface Water Explorer's maximum inundation layer during the past 40 years, Pekel et al. (2016)). Floodplain has only one inlet that is close to *KC* (<10 km downstream from *KC*). The floodplain channel permanently connects the river with the floodplain and has ~ 40 m width on average close to the inlet (Fig. 1A). Therefore, the Mekong River's *WL* (and *Q*) around the inlet determines the amount of hydrological input fluxes entering the floodplain. Prior to 2000, daily *Q* and *WL* at *KC* showed a relatively consistent trend without a change after the MK test (p-value = 0.22 for *WL*). However, *Q* and *WL* showed a decreasing trend after 2000 (p-value < 0.01). The mean annual water level has decreased from 6.94 (pre-2000) to 6.56 m (post-2000). This might be related to the operation of the dams in the Mekong upstream as most of them were built after 2000 (11 out of 12 on the main channel), with many more planned to be built in the near future in the upstream reaches from Cambodia (Hecht et al. 2019; Latrubesse et al. 2020). The impact of the upstream dams is also evident in surface suspended sediment concentration time series estimated at *KC* (Fig. 3E), showing a decreasing trend (p-value < 0.01). When compared pre-dam with post-dam, the monthly averaged *SSSC* decreased from 70.3 to 60.6 mg/l at *KC* (Fig. 3H), approximately a 14% decrease. In summary, *Q*, *WL* and *SSSC* at *KC* all showed a decreasing trend since the 1980s, which could have been attributed to the upstream dam construction and operation activities.

The daily discharge observed at the outlet station *NL*, on the other hand, showed no significant trends overall when assessed over the 40 years (1980–2020, p-value = 0.07). However, a decreasing trend in WL is present when the time series is divided into two periods (before vs after 2000, p-value < 0.01). In the case of *NL*, we attribute the trend mainly to not only the upstream dams but also the aggressive riverbed mining activities taking place in this area (which is not as much in the case of *KC*). However, it should be noted that it is very challenging to provide clear evidence of the dam due to the complex hydrological interactions of the Mekong River with the Tonle Sap Lake that largely alters the Mekong's hydrology downstream of *PPP* (Kummu et al., 2014). Rather we speculate that the impact of riverbed mining around the reach between *PPP* and *NL* could have more significantly affected the observed decreasing trend of *WL* after 2000. This reach is one of the most intensively mined area in the Mekong River (Hackney et al., 2020; Ng & Park, 2021). Since the effect of riverbed mining is localized, dredging may result in the incision of the riverbed, which lowers the water level without drastically altering the *Q* at the same place as observed in the Mekong Delta (Park et al., 2020). *SSSC* also decreased substantially since 1987 at *NL* (p-value < 0.01), from a mean annual average of 53.1 to 47.2 mg/l (~12% decrease) before and after 2000, respectively.

The floodplain annual water budget calculated using Eq.1 in Section 2.2 was analyzed. $Q_{Outlet2}$, representing the annual water loss through

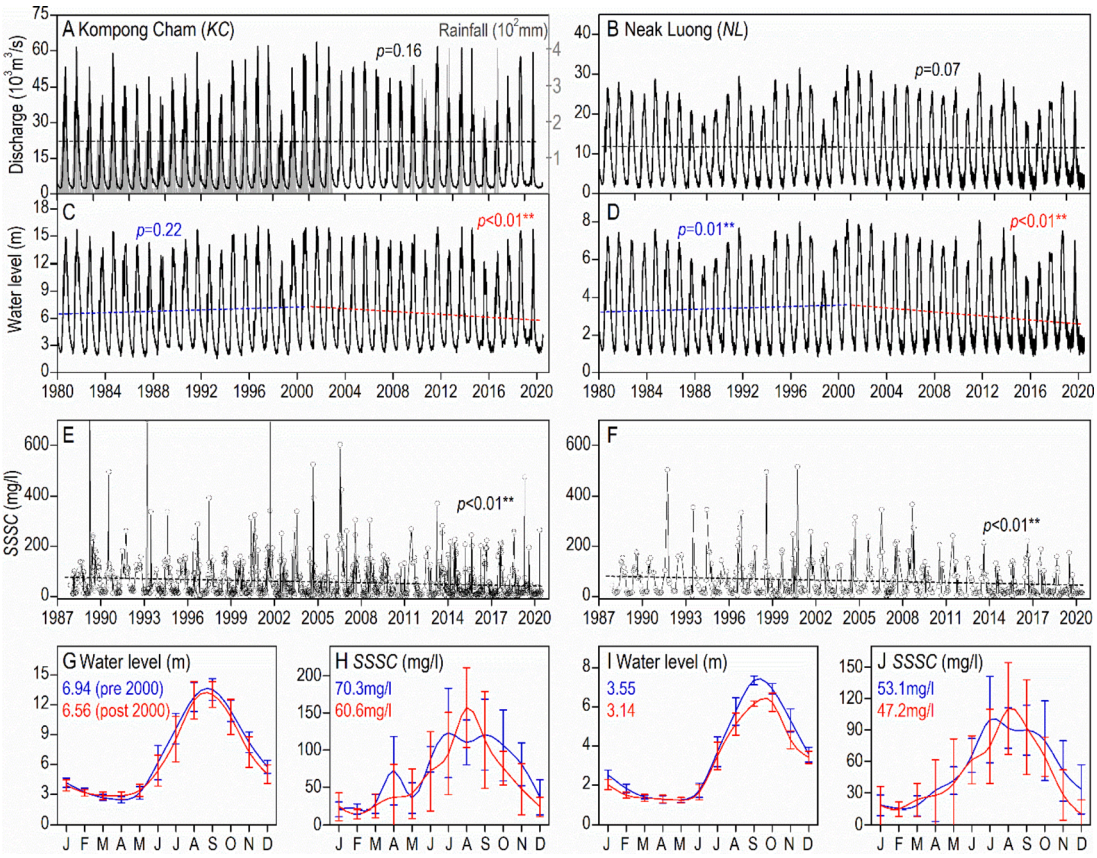

Fig. 3. Hydrological trends of analyzed gauge stations. A-F: Hydrological data (Discharge, water level and estimated suspended sediment concentration (*SSSC*)) at the two most important stations: Kompong Cham (*KC*) and Neak Luong (*NL*). Total monthly rainfall at *KC* is also presented (grey). *p*-values indicate the statistical significance after the Mann-Kendall test of the time series. G-J: Monthly averaged water level and *SSSC* (and their standard errors) for the two periods: pre-2000 and post-2000, for the two stations.

this floodplain channel, was estimated to be almost negligible: <40 m^3/s (mean annual discharge) which is<1% of the mean annual discharge of the Mekong at *NL*. The total annual rainfall was computed to be 2.65x10^9 m^3 on an inter-annual average. The annual water budget over the investigated period (1980–2020) was around 31.4x10^3m^3, with the highest and lowest of 83.1 x10^3m^3 and 3.27x10^3m^3 observed in 1983 and 2002, respectively. The overall increasing trend since 1980 was statistically significant (p-value < 0.01 and Sen's slope = 0.0137). Given that the WLs at the floodplain inlet (as well as in the outlet) decreased significantly, particularly after 2000 (Fig. 3D), which should have decreased the river-floodplain connectivity and the floodplain recharge through the inlet, it is remarkable to observe that the floodplain water budget has increased over time. Looking at the seasonal distribution of the floodplain water storage, a good part of the annual water storage

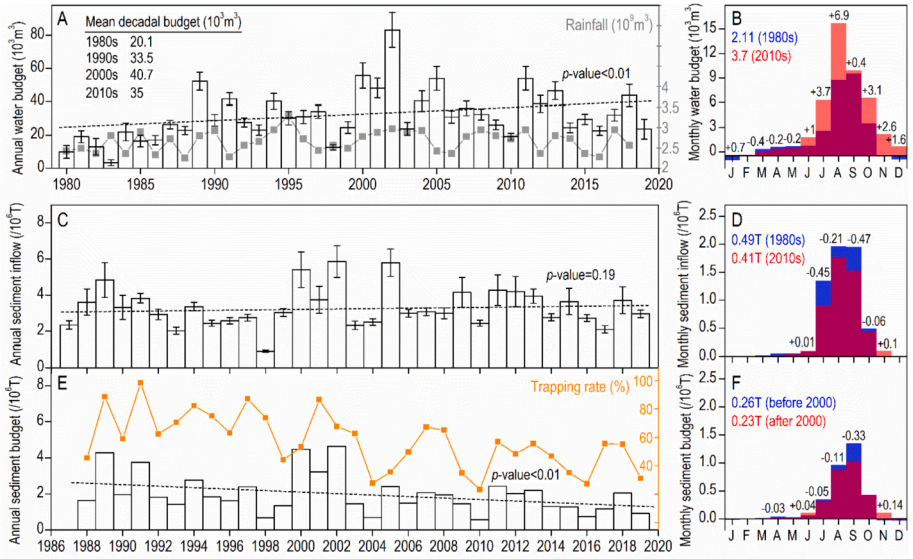

Fig. 4. Floodplain water and sediment budget. A and B: Annual and monthly water storage budgets of the floodplain since 1980, respectively. Total annual rainfall (in volume) landed on the floodplain calculated from the daily rainfall gauge at KC (total annual × floodplain area) is shown. C and D: Annual and monthly sediment inflow of the floodplain since 1980, respectively. E and F: Annual and monthly sediment storage budget of the floodplain, respectively. Sediment trapping rate is computed as the annual sediment budget/sediment inflow.

happens during the rising season when the floodplain has been recharged with the river water (Fig. 4B). Approximately 91 and 84% of the annual water budget (i.e. 25 and $39x10^3m^3$ volume) have been stored during the four months (July to October) for the periods the 1980s and the 2010s, respectively. Comparing these two periods, most of the months presented an increased water monthly budget, with the highest increases of 6.9×10^3 m^3 and 3.7×10^3 m^3 observed in July and August, respectively (Fig. 4B).

We also took notice that although the floodplain's annual water budget has increased since the 1980s, the annual sediment inputs from the Mekong River to the floodplain in the same period does not exhibit any significant trends of shifts, as shown in Fig. 4C. This is likely due to the dam-induced decrease of *SSSC* in the Mekong River around *KC* that has offset the effect of increased floodplain water recharge. Despite some outliers, such as the exceptionally high values associated with 2002 and 2005 and the low values in 1998, the overall inter-annual average remained around $3x10^6T$ without any significant trends (p-value = 0.19). The comparison of the annual sediment inflows between the earliest and the latest investigated decades (the 1980s vs 2020s) reveals a slightly decreasing trend of -0.45 and $-0.19x10^6T$ during the months of July and August when the water level at the Mekong is at its peak; however, the mean monthly inflows of the two decades remained relatively similar (i.e., 0.49 to $0.41x10^6T$) (Fig. 4D). Likewise, to the annual water budget, floodplain sediment input from the Mekong has substantially concentrated during the rising season, particularly close to the peak water stages in the Mekong River around July to September.

Intriguingly, against the stationary trend of the floodplain sediment inflows (even though discharge has increased over the same period), the annual floodplain sediment budget has significantly decreased (1988–2020, p-value < 0.01), as revealed in Fig. 4E. More specifically, the average sediment budget before 2000 was $2.1x10^6T$, while it decreased by approximately 30% to $1.46x10^6T$ (2010–2020). Phasing with the sediment inflows, most of the sedimentation in the floodplain occurred close to the peak stage around August and September on an inter-annual average (Fig. 4F). Finally, the sediment trapping rate of the floodplain showed a clear decreasing trend during the investigated period, ranging from 98% (1991) to around 23% (2010). This indicates that the role of the floodplain as a sediment sink has been diminishing gradually over the past 40 years and that a substantial portion of the Mekong's sediment entering the floodplain currently flows back to the river through the outlets. We would like to remark that the observed decreasing patterns of floodplain sediment budget occurred while the floodplain sediment inflows have not considerably changed over the same period (since the 1980s). This incongruous behaviour of the floodplain seems to be enabled through the gradual decrease of the trapping rate in the floodplain (in which the causes are discussed in the next section).

3.2. Floodplain hydrology and agricultural expansion

There are many other possible causes for the incongruous hydrological developments presented in this paper, yet here we focus on only one anthropogenic activity. More specifically, we could have associated the increased annual water budget in the floodplain with the agricultural expansion in the floodplain for a couple of reasons. First, since the 1980s, the floodplain has experienced drastic land-use change – paddy field area has increased approximately 300% from 457 to 1,381 km^2 (out of around 2,200 km^2 total floodplain area), while the natural vegetation cover has decreased from 861 to 343 km^2 (approximately −39%) (Fig. 1D and E and Fig. 5A and B). The area of the seasonally flooded land in the floodplain has also increased from 1,878 (1985–1995) to 2,238 (1996–2020) km^2, based on the data by Pekel et al. (2016) (Fig. 1 A and B). Second, most of the increased/newly generated seasonally flooding parts of the floodplain are irrigated farmlands that have been converted from the natural vegetation (forest and shrubs). Overall, the mean annual water extent has drastically increased in the floodplain since the 1980s (p-value < 0.01 and $R^2 = 0.4$, Fig. 1C. Combining this water extent time series with the floodplain water budget (volume), we roughly estimated the mean depth of the flooding during the peak stage. We used the annual water extent maxima and monthly water budget for August and September (from Fig. 4B and estimated the mean depth (using water volume in m^3 divided by area in m^2) for the 1980s and 2000s as 0.82 and 1.64 m respectively, indicating the increase in the flood water depth over time.

Here we remark on the two key drivers for the floodwater depth increase in the floodplain: surface erosion and land subsidence. The floodplain has also experienced a rapid expansion of the paddy fields (Fig. 5B). Similar trends were also observed around the Tonlé Sap region, where naturally forested areas have been rapidly converted to paddy fields for rice cultivation to fuel the country's economic development (KC et al., 2019). Evidently, such rapid intensification of agriculture came with a hefty price. Several pristine landscapes, including the indigenous vegetated areas of the floodplain, as shown in Fig. 5E, have been compromised. Hydrologically, the "non-heterogeneous" paddies are much smoother than the naturally "rugged" vegetated landscapes, hence the larger velocity of the overland flows of the former

Fig. 5. Field pictures from the floodplain. A: Natural vegetation of wetland in Prey Veng Province, Cambodia B: Rice paddy field in Prey Veng Province, Cambodia ((Photo credit Lim Nary from https://www.khmertimeskh.com/) C: Erosional surface showing runoffs incised into small gullies after rainfall, where it used to be colonized by primary vegetation (Pheng et al., 2019) (photo courtesy of Yuji Kohgo). D: House damage due to land subsidence in Kandal Province (https://dap-news.com/international/2020/10/17/90703/).

condition. The conversion of landscape as such, in turn, implies a duo-impact, (i) bypassing: sediments originating from upstream now have a smaller chance of settling in the floodplain, and (ii) erosion: topsoil that originated from the vegetated landscape will be eroded. Fig. 5C provides an example of the surface erosion in the Kandal Stung district, Kandal province. This was also verified by our modelling results presented in the next section.

Another cause is the land subsidence due to intensive groundwater extraction which is the widely recognized issue across Cambodia (Chen et al., 2019; Erban et al., 2014; Minderhoud et al., 2018). Provinces around Mekong River close to *PPP* where the nation's population is concentrated (such as Phnom Penh, Kandal and Prey Veng), dependency on the groundwater usage mainly for agriculture and domestic purposes, such as drinking or cooking is substantial, with typical extraction rates over 35,000 m^3 per day in each province (data from the 1990s and 2000s, Fig. 6A. In these provinces, groundwater comprises over 90% of the total domestic water use (Fig. 6B). In our study area (Kandal province), double cropping is a widely adapted agricultural practice, where farmers exploit groundwater to irrigate crops (mostly paddy fields) during the dry season when floodplain recharges from both the rainfall and the Mekong water is limited (IRRA, 2010; Kwak et al., 2015; Ear et al., 2017).

NDVI time series mapped during the dry season also shows an increasing trend since 1978 (p-value < 0.01 and $R^2 = 0.32$, Fig. 6D, indicating that the irrigation for the dry season cropping in the floodplain has been intensified over time. The groundwater level time series from the two monitoring (*P.24* and *P.15*, 1996–2008) wells in the province also showed a significant decreasing trend of 51 and 49 cm/year, respectively. This could have served as a proxy of the land subsidence due to the soil compaction (Fig. 6E). In fact, the groundwater drawdown rates are exceeding the natural compaction rate of soil and comparable to the upper limits of anthropogenic-driven groundwater level decrease observed throughout the Indochina Peninsular. For example, groundwater level declines between 2.5 and 50 cm/year in Hanoi and 30 cm/year in the Vietnamese Mekong Delta (Erban et al., 2014; Tam and Nga, 2018). We also present field observations of surface sinking in the Kandal that relative level of ground has subsided after intensive groundwater drawdown (Fig. 5D). In summary, it is evident that the floodplain land has been lowered, mainly due to the dry season irrigation driven by the agricultural expansion in the floodplain as well as surface erosion in the recent decades.

We consider that agricultural expansion-driven lowering of the floodplain landscape due to surface erosion and land subsidence has increased the floodplain's seasonal water storage. Although the *SSSC* in the Mekong has decreased over time, floodplain sediment recharge remained stationary. Ironically, the annual floodplain sediment budget has decreased, which can be explained only by the decrease in the trapping rate. Currently, the floodplain traps about 40% (after 2010) of the sediment entering the floodplain, and the lowest rate around 23% was observed in 2010; this rate used to be around 65% in the late 1980s. The floodplain is changing into a sediment bypassing system (instead of an efficient sink). We conclude that the floodplain trapping rate has been affected dramatically by the land cover change in the floodplain, which altered the surface roughness controlling the flow resistance and sedimentation. Large scale conversion of natural and pioneer vegetation to paddy fields or other low-lying crops in the floodplain should have considerably reduced the roughness of the terrain by hampering settlement of the sediment from the river.

3.3. Floodplain sedimentation patterns and hydraulic impacts on inundation dynamics

Although the budgetary approach adopted in this study was mostly based on the river gauge stations data, the patterns of sedimentation within the floodplain remain unknown. To quantitatively assess the sedimentation patterns in the floodplain under different terrain roughness conditions (that has been described in Section 3.2), here we show hydrodynamic simulation results. First, we show the validation result of the model set up. We compared the *SSSC* map simulated over the floodplain in the three distinct phases (rising, peak and falling stages) in 2000 to the *SSSC* time series estimated from field-calibrated Landsat images (i.e. observed) (Fig. 7). Out of 30 randomly distributed validation points, Landsat-driven *SSSC* maps yielded at least 25 sample points to validate after filtering out the cloud, shadow and other unqualified pixels. The validation results yielded the average RMSE of 28.9 mg/l without a notable seasonal dependency (Fig. 7B). The RMSE indicates a

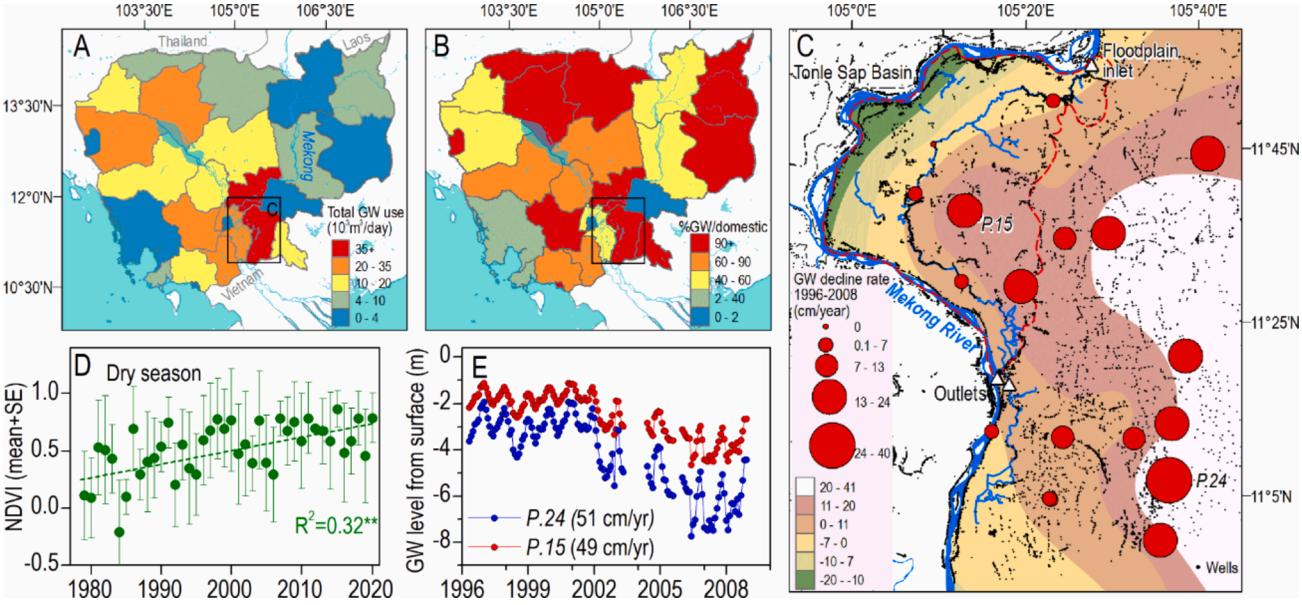

Fig. 6. Groundwater data results. A: Daily total groundwater (GW) drawdown rates per province in Cambodia. B: Percentage of the groundwater usage out of total domestic water use, i.e. GW dependency. C: Annual decline rate between 1996 and 2008 of the groundwater levels measured from the 17 monitoring wells within and around the floodplain. Ordinary Kriging is used for interpolation to estimate a continuous surface GW drawdown rate. Also, the groundwater wells are shown (data from the World Bank at cambodiawellmap.com). D: Dry season NDVI (mean and standard error) mapped over the floodplain since 1980. E: Time series groundwater level from the surface for the two stations: *P.24* and *P.15* (estimated).

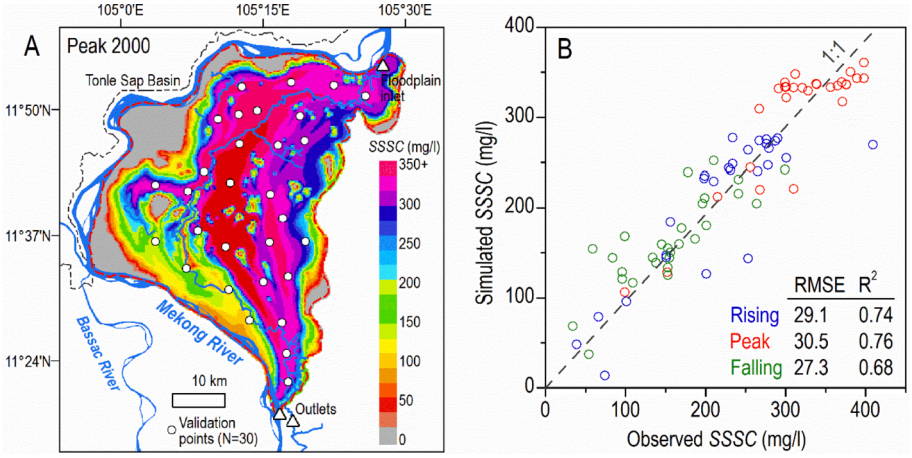

Fig. 7. Numerical model validation. A: Surface suspended sediment concentration (*SSSC*) map during the peak flow of 2000 simulated from the 2D hydrodynamic model and the validation points (N = 30) across the floodplain. B: Validation results of the modeling using the *SSSC* time series computed from the field-calibrated Landsat data. Validation has been conducted for the three distinct seasons (rising, peak and falling) in 2000.

reasonably good performance of the hydrodynamic simulation, as it is lower than 10% of the total *SSSC* variability across the floodplain (ranging from 30 to ~ 400 mg/l). Likewise, an average R^2 across the seasons also yielded a satisfactory value of 0.73, with the highest (0.76) and the lowest (0.68) fits during peak and falling seasons, respectively.

When the river water enters the floodplain through the floodplain channel via an inlet, it seems that the sedimentation along the floodplain channel is not high (<0.5 cm/year) (Fig. 8). This is perhaps due to the limited vertical aggradation capacity of the floodplain channel, associated with the recent decrease in *SSSC* and the lowering of water level in the Mekong River around *KC* (Fig. 3). The levee height of the floodplain channel seems low, as inferred from the observation that every season they are fully covered by water during the peak flood stage (observation from Pekel et al., (2016)). The floodplain landscape is also generally flat (average slope ~ 4 cm/km) with rounded lakes and extensive paddy fields that are hydrologically well-connected through small-medium sized irrigation canals. These canals act as a conveyor to transport sediment throughout the floodplain (and to the distal parts of the floodplain during the flood season). Therefore, the sedimentation rate seems to be not in phase with the distance to the channel due to well-developed channelized connections, as opposed to the other typical flood-pulse system (Junk et al., 1989). Similar floodplain internal connectivity patterns have been observed in other pristine floodplain lakes that due to channelized network in the floodplain, routing of the river flood water presents intricate network patterns (Park & Latrubesse, 2017).

The spatial distribution of sedimentation in the floodplain is heterogeneous. The rates range from nearly 0 up to around 8 cm/year, in the case of large rounded lakes developed through continuous overbank dispersion from the floodplain channel. They are concentrated in the western part of the floodplain and can have about 3 cm/year of sedimentation on average. These lakes are proximal to the river but indirectly receive water from the Mekong via the floodplain channel that starts from the inlet. Overall, the sedimentation rate for a good part of the floodplain (more than 80% area) showed <0.4 cm/year, and sedimentation hotspots correlate with the location of the rounded lakes (locally depressed) along the floodplain channel. In other large rivers, they are called 'impeded floodplain lakes' and have been described as important sediment sinks within floodplain (Park, 2020; Park & Latrubesse, 2019). It is assumed that most of the deposited materials are fine

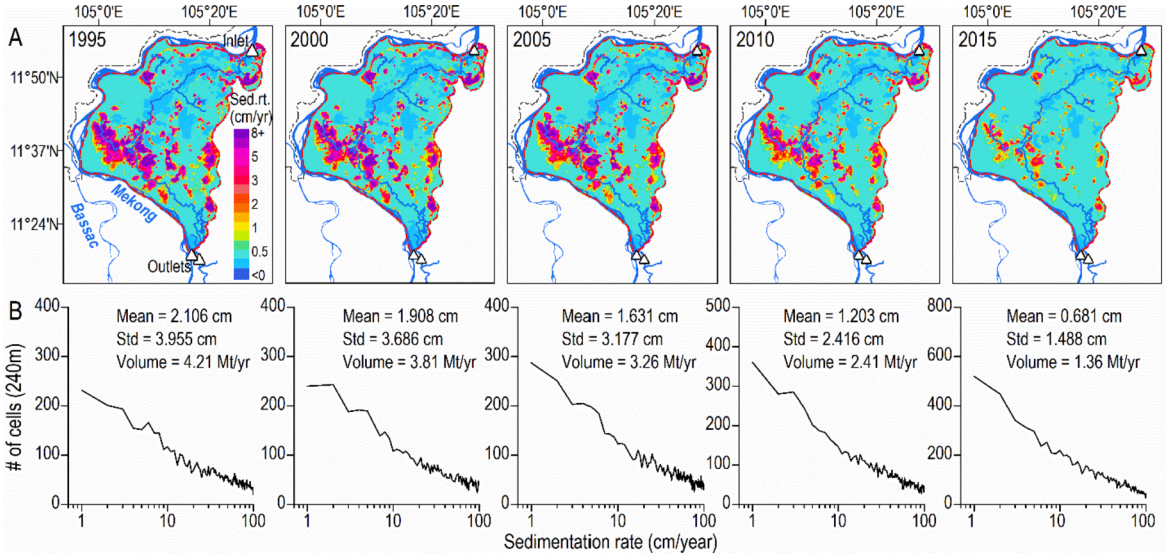

Fig. 8. Numerical model simulation results. A: Hydrodynamic simulation results of the annual sedimentation rate (cm/year) in floodplain over the 5 periods (1995 to 2015). B: Image histogram of the sedimentation map for each period and their statistics (mean and standard deviation). Mean flow velocity (0.226, 0.224, 0.252, 0.250, and 0.215 cm/s in 1995, 2000, 2005, 2010, and 2015, respectively) within the floodplain and the total annual sedimentation volume has been computed.

cohesive sediments (washload), which are exhaustively sourced from the river. Our grain size distribution analysis results at the lower reach of the Mekong also indicated that suspended sediment is mostly silty and clay materials and <5% of the sandy fractions (Fig. 2). Given that the freeboard of the Mekong at *KC* is <10 m and the exponentially decaying nature of the sandy sediment concentration as it gets toward the river surface, it is not likely that suspended sandy loads enters the floodplain even during the flood (mean depth and velocity of the Mekong around *KC* during flood season were >20 m and <1.5 m^3/s respectively) (Hackney et al., 2020).

Impacts of land cover change on sedimentation rate on floodplain was remarkable, shown from our simulation results of the floodplain sedimentation over the five different years (1995 to 2015 with 5-years interval) (Fig. 8). Along with the agricultural expansion, overall sedimentation rates across the floodplain decreased with the pronounced decrease observed around the rounded lakes in the western fringe. We consider that though a similar amount of sediment fluxes enters the floodplain (on inter-annual average, Fig. 4C, the floodplain cover has gradually lost the capacity to trap sediment due to the decreased terrain roughness. Therefore, it is assumed that currently, these rounded lakes efficiently export sediments mostly during the peak and falling seasons. Our modelled sedimentation rates showed a decreasing trend from 2.11 (1995) to 0.68 cm/year (2015) on average, which translates into the sediment deposited mass of 4.21 and 1.36 Mt, respectively. When converted to the volume using an aggregate density of 1.6 t/m^3 (Binh et al., 2020a), they were 2.63 and 0.85 Mm^3, which are almost in agreement with the volume estimated for the period before 1995 ($2.75x10^6$ m^3) and after 2015 ($1.23x10^6$ m^3) through the budgetary approach (Fig. 4E and F). A slight discrepancy of the modelled budget (from the budget estimated from gauge stations) can be related to the morphological complexity of the floodplain landscape. For example, we could not incorporate the land subsidence factor in the hydrodynamic simulation due to the lack of a subsidence map. In the follow-up study, we expect to generate a subsidence map using Interferometric Synthetic Aperture Radar (InSAR), which can be used to improve the hydrodynamic simulation accuracy.

4. Summary and final remarks

In this paper, we address the patterns of floodplain water and sediment budget in the floodplain of the Mekong based in Cambodia over the past 40-years. Both the surface suspended sediment concentration and water level in the Mekong River decreased due to upstream dam constructions and intensive riverbed mining. However, floodplain seasonal water storage increased for the same period, and the rate of sediment input from the river is almost constant during the study period. The annual sediment budget of the floodplain, however, significantly decreased during the same period mainly due to the reduced sediment trapping rate (from 66% in the 1980s to 46% in the 2010s), and a good part of sediment entering the floodplain currently bypass it and enters back into the river. We conclude that this observed paradox was enabled by the agricultural expansion in the floodplain that increased erodibility of the surface and lowered the land.

We expect the findings of our paper are of scientific significance in multiple aspects. *Firstly*, connecting agricultural expansion with the alterations of floodplain's water and sediment budget constitutes an unexplored environmental consequence of human activities in the lower Mekong River. *Secondly*, the hydrological patterns of a large lowland floodplain described in this study has never been reported before or elsewhere in the world, whereby three different hydro-geomorphological processes happen simultaneously: (1) increased water budget, (2) constant sediment inflows, and (3) decreased sediment budget. *Lastly*, this study was able to contribute novel insight into understanding the sediment balance situation along the broader Mekong River. We speculate that lowered sediment trapping in the Cambodian floodplain might have partially contributed to alleviating the sediment deficit downstream at the Vietnam Mekong Delta. However, such floodplains, while losing one of their most fundamental functions as "sinks of sediments", cannot evolve geomorphologically, thus would remain "incomplete" indefinitely.

CRediT authorship contribution statement

Edward Park: Conceptualization, Funding acquisition, Project supervision, Data processing, Writing - original and revised. **Huu Loc Ho:** Conceptualization, Data acquisition, Data processing, Writing - original and revised. **Doan Van Binh:** Data acquisition, Data processing, Writing - original and revised. **Sameh Kantoush:** Data acquisition, Data processing, Writing - original and revised. **Danielle Poh:** Data processing, Writing - original and revised. **Enner Alcantara:** Data acquisition, Data processing, Writing - original and revised. **Sophal Try:** Data acquisition, Data processing, Writing - original and revised. **Yunung Nina Lin:** Data acquisition, Data processing, Writing - original and revised.

Declaration of Competing Interest

The authors declare that they have no known competing financial interests or personal relationships that could have appeared to influence the work reported in this paper.

Acknowledgments

This study is funded by the National Institute of Education at the Nanyang Technological University (SUG-NAP EP3/19), Ministry of Education of Singapore (AcRF Tier1 RT 06/19, AcRF Tier1 MOE:2021-T1-001-056, AcRF Tier2 02A-2020) and National Science Foundation of USA (#1558446). CHIRPS Data was downloaded and processed from the Climate Hazards Centre, UC Santa Barbara (https://data.chc.ucsb.edu/products/CHIRPS-2.0/).

References

Binh, D.V., Kantoush, S., Sumi, T., 2020a. Changes to long-term discharge and sediment loads in the Vietnamese Mekong Delta caused by upstream dams. Geomorphology 353, 107011.

Binh, D.V., Wietlisbach, B., Kantoush, S., Loc, H.H., Park, E., Cesare, G.D., Cuong, D.H., Tung, N.X., Sumi, T., 2020b. A Novel Method for River Bank Detection from Landsat Satellite Data: A Case Study in the Vietnamese Mekong Delta. Remote Sensing 12 (20), 3298.

Binh, D.V., Kantoush, S.A., Sumi, T., Mai, N.P., Trieu, N.A., La, T.V., Tran, A.D., 2021. Effects of riverbed incision on the hydrology of the Vietnamese Mekong Delta. Hydrol. Process. 35, e14030.

Breiman, L. (1999). Random forests. UC Berkeley TR567.

Chen, F., Guo, H., Ishwaran, N., Liu, J., Wang, X., Zhou, W., Tang, P., 2019. Understanding the relationship between the water crisis and sustainability of the Angkor World Heritage site. Remote Sens. Environ. 232, 111293.

Cramb, R., Sareth, C., Vuthy, T., 2020. The commercialization of rice farming in Cambodia. In: White gold: the commercialization of rice farming in the lower Mekong Basin. Palgrave Macmillan, Singapore, pp. 227–245.

Doxaran, D., Froidefond, J.M., Castaing, P., 2002. A reflectance band ratio used to estimate suspended matter concentrations in sediment-dominated coastal waters. Int. J. Remote Sens. 23 (23), 5079–5085.

Ear S., Sim S., Chhim C., & Khiev P (2017). Rice Policy Study: Implications of Rice Policy Changes in Vietnam for Cambodia's Rice Policy and Rice Producers in South Eastern Cambodia. *CDRI Working Paper Series* No. 113. Phnom Penh: CDRI.

Erban, L.E., Gorelick, S.M., Zebker, H.A., Fendorf, S., 2013. Release of arsenic to deep groundwater in the Mekong Delta, Vietnam, linked to pumping-induced land subsidence. Proc. Natl. Acad. Sci. 110 (34), 13751–13756.

Erban, L.E., Gorelick, S.M., Zebker, H.A., 2014. Groundwater extraction, land subsidence, and sea-level rise in the Mekong Delta, Vietnam. Environ. Res. Lett. 9 (8), 084010.

Erban, L.E., Gorelick, S.M., 2016. Closing the irrigation deficit in Cambodia: Implications for transboundary impacts on groundwater and Mekong River flow. J. Hydrol. 535, 85–92.

Eslami, S., Hoekstra, P., Trung, N.N., Kantoush, S.A., Van Binh, D., Quang, T.T., van der Vegt, M., 2019. Tidal amplification and salt intrusion in the Mekong Delta driven by anthropogenic sediment starvation. Sci. Rep. 9 (1), 1–10.

Exner, F.M., 1920. Zur Physik der Dünen. Akad. Wiss. Wien Math. Naturwiss. Klasse 129, 929–952.

Exner, F.M., 1925. Über die Wechselwirkung zwischen Wasser und Geschiebe in Flüssen. Akad. Wiss. Wien Math. Naturwiss. Klasse 134, 165–204.

FAO. (2015). New GEF project in preparation to improve sustainable use and governance of groundwater in Cambodia-Mekong River Delta Transboundary Aquifer. From http://www.fao.org/cambodia/news/rss/detail-events/en/c/1307818/ (Retrieved 23 March 2021).
Funk, C., Peterson, P., Landsfeld, M., Pedreros, D., Verdin, J., Shukla, S., Michaelsen, J., 2015. The climate hazards infrared precipitation with stations—a new environmental record for monitoring extremes. Sci. Data 2 (1), 1–21.
Hackney, C.R., Darby, S.E., Parsons, D.R., Leyland, J., Best, J.L., Aalto, R., Houseago, R. C., 2020. River bank instability from unsustainable sand mining in the lower Mekong River. Nat. Sustainability 3 (3), 217–225.
Hecht, J.S., Lacombe, G., Arias, M.E., Dang, T.D., Piman, T., 2019. Hydropower dams of the Mekong River basin: A review of their hydrological impacts. J. Hydrol. 568, 285–300.
Helsel, D. R., & Hirsch, R. M. (1992). Statistical methods in water resources (Vol. 49). Elsevier.
Hung, N.N., Delgado, J.M., Güntner, A., Merz, B., Bárdossy, A., Apel, H., 2014. Sedimentation in the floodplains of the Mekong Delta, Vietnam. Part I: suspended sediment dynamics. Hydrol. Process. 28, 3132–3144.
International Development Enterprises (iDE) (2005). Final Report: Strategic Study of Groundwater Resources in Prey Veng and Svay Rieng (Phase 1). Phnom Penh: iDE.
Johnston, R., Reberts, M., Try, T., 2013. Groundwater for irrigation in Cambodia. Issue brief, IWMI.
Junk, W.J., Bayley, P.B., Sparks, R.E., 1989. The flood pulse concept in river-floodplain systems. Canadian special publication of fisheries and aquatic sciences 106 (1), 110–127.
KC, K. B., Seng, R., & Fraser, E. (2019). Should I stay or should I go? Fishers' ability and willingness to adapt to environmental change in Cambodia's Tonlé Sap Lake. *Fisheries Management and Ecology*, 26(3), 211-223.
Kummu, M., Tes, S., Yin, S., Adamson, P., Józsa, J., Koponen, Richey, J.& Sarkkula, J. (2014). Water balance analysis for the Tonle Sap Lake–floodplain system. *Hydrological Processes*, 28(4), 1722-1733.
Kwak, Y., Shrestha, B.B., Yorozuya, A., Sawano, H., 2015. Rapid damage assessment of rice crop after large-scale flood in the cambodian floodplain using temporal spatial data. IEEE J. Sel. Top. Appl. Earth Obs. Remote Sens. 8 (7), 3700–3709.
Latrubesse, E.M., Park, E., Sieh, K., Dang, T., Lin, Y.N., Yun, S.H., 2020. Dam failure and a catastrophic flood in the Mekong basin (Bolaven Plateau), southern Laos, 2018. Geomorphology 362, 107221.
Loc, H.H., Diep, N.T.H., Can, N.T., Irvine, K.N., Shimizu, Y., 2017. Integrated evaluation of Ecosystem Services in Prawn-Rice rotational crops. Vietnam. *Ecosystem Services* 26, 377–387.
Loc, H.H., Van Binh, D., Park, E., Shrestha, S., Dung, T.D., Son, V.H., Truc, N.H.T., Mai, N.P., Seijger, C., 2021a. Intensifying saline water intrusion and drought in the Mekong Delta: From physical evidence to policy outlooks. Sci. Total Environ. 757, 143919.
Loc, H.H., Park, E., Thu, T.N., Diep, N.T.H., Can, N.T., 2021b. An enhanced analytical framework of participatory GIS for ecosystem services assessment applied to a Ramsar wetland site in the Vietnam Mekong Delta. Ecosyst. Serv. 48, 101245.
Loc, H.H., Low Lixian, M., Park, E., Dung, T.D., Shrestha, S., Yoon, Y.J., 2021c. How the saline water intrusion has reshaped the agricultural landscape of the Vietnamese Mekong Delta, a review. Sci. Total Environ. 794, 148651.
Lu, X., Kummu, M., Oeurng, C., 2014. Reappraisal of sediment dynamics in the Lower Mekong River. Cambodia. *Earth Surface Processes and Landforms* 39 (14), 1855–1865.
Manning, R., Griffith, J.P., Pigot, T.F., Vernon-Harcourt, L.F., 1890. On the flow of water in open channels and pipes. Transactions of the Institution of Civil Engineers of Ireland. 20, 161–207.
Masek, J.G., Vermote, E.F., Saleous, N., Wolfe, R., Hall, F.G., Huemmrich, K.F., Gao, F., Kutler, J., Lim, T.K., 2012. LEDAPS Landsat calibration, reflectance, atmospheric correction preprocessing code. ORNL DAAC.
McBride, G.B., 2005. Using statistical methods for water quality management: issues, problems and solutions, Vol. 19. John Wiley & Sons.
Minderhoud, P.S.J., Coumou, L., Erban, L.E., Middelkoop, H., Stouthamer, E., Addink, E. A., 2018. The relation between land use and subsidence in the Vietnamese Mekong delta. Sci. Total Environ. 634, 715–726.
Ng, W.X., Park, E., 2021. Shrinking Tonle Sap and the recent intensification of sand mining in the Cambodian Mekong River. Sci. Total Environ. 146180.
Pablo, T., 2018. Sysyphe User Manual. Version 7 (3), 70.
Park, E., Latrubesse, E.M., 2014. Modeling suspended sediment distribution patterns of the Amazon River using MODIS data. Remote Sens. Environ. 147, 232–242.
Park, E., Latrubesse, E.M., 2017. The hydro-geomorphologic complexity of the lower Amazon River floodplain and hydrological connectivity assessed by remote sensing and field control. Remote Sens. Environ. 198, 321–332.
Park, E., Latrubesse, E.M., 2019. A geomorphological assessment of wash-load sediment fluxes and floodplain sediment sinks along the lower Amazon River. Geology 47 (5), 403–406.
Park, E., 2020. Characterizing channel-floodplain connectivity using satellite altimetry: Mechanism, hydrogeomorphic control, and sediment budget. Remote Sens. Environ. 243, 111783.
Park, E., Ho, H.L., Tran, D.D., Yang, X., Alcantara, E., Merino, E., Son, V.H., 2020. Dramatic decrease of flood frequency in the Mekong Delta due to riverbed mining and dyke construction. Sci. Total Environ. 723, 138066.
Park, E., Loc, H.H., Van Binh, D., Kantoush, S., 2021a. The worst 2020 saline water intrusion disaster of the past century in the Mekong Delta: Impacts, causes, and management implications. Ambio 1–9.
Park, E., Lim, J., Ho, H.L., Herrin, J., Chitwatkulsiri, D., 2021b. Source-to-sink sediment fluxes and budget in the Chao Phraya River, Thailand: A multi-scale analysis based on the national dataset. J. Hydrol. 125643.
Pekel, J.F., Cottam, A., Gorelick, N., Belward, A.S., 2016. High-resolution mapping of global surface water and its long-term changes. Nature 540 (7633), 418–422.
Pheng, S., Hori, T., Kohgo, Y., 2019. Erosion of irrigation facilities in Cambodia paddy farming region and the measures for protection. Paddy Water Environ, 17 (4), 689–702.
Schwatke, C., Dettmering, D., Bosch, W., Seitz, F., 2015. DAHITI–an innovative approach for estimating water level time series over inland waters using multi-mission satellite altimetry. Hydrol. Earth Syst. Sci. 19 (10), 4345–4364.
Shah, T., Burke, J., Villholth, K. G., Angelica, M., Custodio, E., Daibes, F., Hoogesteger, J., Giordano, M., Girman, J., van der Gun, J, Kendy E., Kijne, J., Llamas, R., Masiyandima, M., Margat, J., Marin, L., Peck, J., Rozelle, S., Sharma, B. R., Vincent, L. & Wang, J. (2007). *Groundwater: a global assessment of scale and significance.*
Sok, C., Choup, S., 2017. Climate change and groundwater resources in Cambodia. J. Groundwater Sci. Eng. 5 (1), 31–43.
Sok, C. (2017). Angkor water crisis. From https://en.unesco.org/courier/2017-april-june/angkor-water-crisis (Retrieved 17 February 2021).
Tam, V.T., Nga, T.T.V., 2018. Assessment of urbanization impact on groundwater resources in Hanoi, Vietnam. J. Environ. Manage. 227, 107–116.
Villaret, C. (2010). SISYPHE 6.0 User Manual. Modelisation des Apports Hydriques et Transferts Hydro-Sedimentaires-Laboratoire National d'hydraulique et Environnement. IRRA. (2010). Crop Area Map of Cambodia in 2010. Phnom Penh: IRRA.
Villaret, C., Hervouet, J.M., Kopmann, R., Merkel, U., Davies, A.G., 2013. Morphodynamic modeling using the Telemac finite-element system. Comput. Geosci. 53, 105–113.
Winkel, L.H., Trang, P.T.K., Lan, V.M., Stengel, C., Amini, M., Ha, N.T., Viet, P.H., Berg, M., 2011. Arsenic pollution of groundwater in Vietnam exacerbated by deep aquifer exploitation for more than a century. Proc. Natl. Acad. Sci. 108 (4), 1246–1251.
Yamazaki, D., Ikeshima, D., Tawatari, R., Yamaguchi, T., O'Loughlin, F., Neal, J.C., Sampson, C.C., Kanae, S., Bates, P.D., 2017. A high-accuracy map of global terrain elevations. Geophys. Res. Lett. 44 (11), 5844–5853.
Zhou, M.C., Ishidaira, H., Hapuarachchi, H.P., Magome, J., Kiem, A.S., Takeuchi, K., 2006. Estimating potential evapotranspiration using Shuttleworth-Wallace model and NOAA-AVHRR NDVI data to feed a distributed hydrological model over the Mekong River basin. J. Hydrol. 327 (1–2), 151–173.